

# Adaptive Frames-Based Denoising of Confocal Microscopy Data

Alberto Santamaría-Pang, Teodor Ş. Bîldea, Ioannis Konstantinidis and Ioannis A. Kakadiaris

**Abstract**—In this paper, we present a novel frames-based denoising algorithm. Using a general result on lifting frames, we construct a non-separable 3D frame capable of robust edge detection. This frame detects edge information by ensemble thresholding of the filtered data. The denoising uses a hysteresis thresholding step and an affine thresholding function, which are filter-adaptive and take full advantage of the threshold bounds. The threshold bounds are statistically determined from the given data for each directional filter. We compare our denoising method with other methods based on separable 3D wavelets and 3D median filtering, and report very encouraging results on applications to both synthetic and real confocal microscopy data.

## I. INTRODUCTION

During acquisition of image and volume data, the characteristics of the employed device produce noise that is embedded in the image. Different devices and acquisition procedures can lead to different accepted noise models, like Gaussian or Poisson additive noise. The goal of denoising is to recover the original image from a noisy image. Current denoising techniques combine suitable filter/transforms and statistical estimation. Typically, the image is transformed, using filters, into a domain where the noise can be identified; statistical estimation is then performed to remove the influence of noise. Dima *et al.* [3] proposed a wavelet denoising method for confocal microscopy imaging that amounts to shrinking wavelet coefficients associated with noise to zero. They subsequently developed a multiscale edge detector based on the 3D wavelet transform [4]. Their technique is based on the *à trous* pyramidal decomposition scheme. It includes a multiresolution validation method to detect edges and to suppress the responses from noise and contrast variations. Denoising based on non-linear anisotropic filtering was proposed by Broser *et al.* [2]. Noise is being averaged along the local axis of the neuron's tubular-wise dendrites in order to maintain morphological structure. The downside of this method is that the structure of fine neurons can be highly corrupted. Kofahi *et al.* [1] described a morphological neuron reconstruction using an adaptive exploratory search at voxel intensity level. Directional filters are used to describe the neuron's morphology, assuming there is no preprocessing. This method is well suited for images with no significant noise or artifacts that can potentially lead to

A. Santamaría-Pang, T.S. Bîldea and I.A. Kakadiaris are with the Computational Biomedicine Lab (formerly known as Visual Computing Lab), Department of Computer Science, University of Houston, TX 77204, USA. I. Konstantinidis is with The Norbert Wiener Center for Harmonic Analysis and Applications, Department of Mathematics, University of Maryland, College Park, MD 20742. This work was supported in part by NIH 5R01EB001048-02.

an improper reconstruction. Building on our previous work [5], in this paper we propose a 3D frames-based denoising method. Our current work refines the methods presented in [5] and complements the existing literature by developing a non-separable multidirectional frame to eliminate noise. In particular, we have developed a non-separable 3D Parseval frame based on a 1D piecewise linear spline tight frame. The resulting filter bank is multidirectional, capable of detecting edges along the main axes and diagonals in the 3D space. The novelty of the denoising algorithm lies in the affine thresholding strategy, which is adapted to the specific filters. Even though we have developed this denoising algorithm for confocal microscopy data, it is a general algorithm that applies to any 3D data with similar noise assumptions.

The remainder of the paper is organized as follows. In Section II we present the method for lifting frames in order to produce new frames. We recall in Section II-A the notion of *Parseval frame* and we briefly describe in Section II-B the mathematical framework used for constructing our filter bank. Section II-C presents the denoising algorithm proposed in this paper. Results using synthetic and real data are presented in Section III.

## II. METHODS

In this section, we describe the mathematical framework of our methods. The filter bank that we will use generates, by considering all possible translations, a Parseval frame for  $\ell^2(\mathbb{Z}^3)$ . Our method is a general one, and it can be used to construct non-separable frames in any dimension  $d$  ( $d \geq 2$ ). Let us recall that a *digital filter* is a vector  $K \in \ell^2(\mathbb{Z}^d)$  for which the Fourier transform  $k$  is a bounded function. This filter acts on a digital signal by the convolution operator  $C_K$ , defined as  $C_K(s) = s * K$ ,  $s \in \ell^2(\mathbb{Z}^d)$ . On  $\ell^2(\mathbb{Z}^d)$  we will also consider the translation operator  $T_{\mathbf{n}}$ , defined by  $T_{\mathbf{n}}s(\mathbf{m}) = s(\mathbf{m} - \mathbf{n})$ , for every  $\mathbf{n}, \mathbf{m} \in \mathbb{Z}^d$  and  $s \in \ell^2(\mathbb{Z}^d)$ .

### A. Construction of the 3D Parseval Frame

A *frame* in a Hilbert space  $H$  is a collection of vectors  $\{v_i\}_{i \in I} \subset H$ , which satisfies the frame inequalities:

$$A\|x\|^2 \leq \sum_{i \in I} |\langle x, v_i \rangle|^2 \leq B\|x\|^2, \text{ for all } x \in H,$$

where  $A \leq B$  are positive constants called frame bounds. For our purposes,  $I$  is a countable index set. A *Parseval frame* is a frame for which  $A = B = 1$ ; for these frames the inequality above becomes the well-known Parseval identity. Parseval frames have the advantage that they behave as orthogonal bases: the same vectors that are used in

the analysis (decomposition) can be used in the synthesis (reconstruction). We will construct a Parseval frame for the Hilbert space  $\ell^2(\mathbb{Z}^3)$ . We begin our construction with the 1D frame described by Ron and Shen [8] as being the simplest example of a compactly supported tight spline frame. The low-pass  $k_0$ , band-pass  $k_1$ , and high-pass  $k_2$  filters, associated with the Riesz scaling function ( $\phi$ ) and two wavelets ( $\psi_1$  and  $\psi_2$ ) are defined as follows:  $k_0(\omega) = \cos^2(\omega/2)$ ,  $k_1(\omega) = i(\sqrt{2}/2)\sin(\omega)$ , and  $k_2(\omega) = \sin^2(\omega/2)$ . Note that

$$|k_0(\omega)|^2 + |k_1(\omega)|^2 + |k_2(\omega)|^2 = 1,$$

for all  $\omega \in [-\pi, \pi)$ . Therefore, the translates  $T_{\mathbf{n}}$  ( $\mathbf{n} \in \mathbb{Z}$ ) of the impulse responses  $\hat{k}_0 = K_0 = (1/4)[1, 2, 1]$ ,  $\hat{k}_1 = K_1 = (1/4)[\sqrt{2}, 0, -\sqrt{2}]$  and  $\hat{k}_2 = K_2 = (1/4)[-1, 2, -1]$  form a 1D Parseval frame for  $\ell^2(\mathbb{Z})$ . Note that  $K_1$  is a first-order singularity detector while  $K_2$  is a second-order singularity detector. To obtain 3D filters, we simply take the 3-folded tensor products of this frame with itself to obtain a separable 3D frame with 27 filters. More precisely:

$$k_{p \cdot 3 + q \cdot 3 + r}(\omega_1, \omega_2, \omega_3) = k_p(\omega_1)k_q(\omega_2)k_r(\omega_3) \quad (1)$$

with  $p, q, r \in \{0, 1, 2\}$ .

### B. Augmentation of the 3D Tight Frame

We focus our attention on the filters  $K_1, K_3, K_9$ , and their impulse responses  $k_1, k_3, k_9$ , respectively. We wish to augment our frame with non-separable filters capable of detecting edges along the main diagonals in 3D space.

We use our previous framework for augmenting tight frames [10]; it follows a general result, the proof of which is based on Lemma 2.5 of Papadakis [6]. Assume that  $K_r$ , with  $r = 0, 1, \dots, R$  is a family of digital filters whose integer translates form a frame for  $\ell^2(\mathbb{Z}^d)$ . For a given positive integer  $Q$ , let  $U$  be a  $2\pi\mathbb{Z}^d$ -periodic  $(Q+1) \times (R+1)$  matrix-valued function whose entries  $(U(\omega))_{q,r}$  are continuous. The matrix multiplication

$$\begin{aligned} U(\omega)(\hat{K}_0(\omega), \hat{K}_1(\omega), \dots, \hat{K}_R(\omega))^t &= \\ &= (\hat{F}_0(\omega), \hat{F}_1(\omega), \dots, \hat{F}_Q(\omega))^t, \end{aligned}$$

defines a new family of digital filters  $F_q$ , with  $q = 0, 1, \dots, Q$ .

*Proposition 1:* *If there exists  $A > 0$  such that for almost every  $\omega \in [-\pi, \pi)^d$  we have  $A\|\mathbf{x}\| \leq \|U(\omega)\mathbf{x}\|$  for all  $\mathbf{x} \in \mathbb{C}^{R+1}$ , then the integer translates of the new family of digital filters  $F_q$ ,  $q = 0, 1, \dots, Q$  also form a frame for  $\ell^2(\mathbb{Z}^d)$ . If, in particular,  $U(\omega)$  is an isometry for almost every  $\omega \in [-\pi, \pi)^d$ , then the resulting and the original frames have the same frame bounds.*

In our case  $R = 26$  and  $Q = 30$ . We choose  $U$  to be a constant matrix implementing an isometry. Table I presents our choice of  $U$  by listing the result of applying the operations associated with the augmentation process. All the other 23 frame elements not listed remain unchanged. The new frame incorporates  $F_1, F_3$ , and  $F_9$ , which contain scalar multiples of the separable original filters. They are operators

TABLE I  
THE AUGMENTATIONS TO THE SEPARABLE FRAME

Part of augmented frame $\hat{F}$	Part of $U(\hat{K}_0(\omega), \dots, \hat{K}_{26}(\omega))^t$
$\hat{F}_1 =$	$\frac{\sqrt{3}}{2}\hat{K}_1$
$\hat{F}_3 =$	$\frac{\sqrt{3}}{2}\hat{K}_3$
$\hat{F}_9 =$	$\frac{\sqrt{3}}{2}\hat{K}_9$
$\hat{F}_{27} =$	$\frac{1}{4}(\hat{K}_9 + \hat{K}_3 + \hat{K}_1)$
$\hat{F}_{28} =$	$\frac{1}{4}(\hat{K}_9 - \hat{K}_3 + \hat{K}_1)$
$\hat{F}_{29} =$	$\frac{1}{4}(\hat{K}_9 + \hat{K}_3 - \hat{K}_1)$
$\hat{F}_{30} =$	$\frac{1}{4}(\hat{K}_9 - \hat{K}_3 - \hat{K}_1)$

able to detect edges parallel to the coordinates axes. This frame incorporates a set of new directions  $F_{27}, F_{28}, F_{29}$  and  $F_{30}$  containing non-separable filters that are tuned along the main diagonals. For example,  $F_{28}$  estimates the directional derivative in the direction of the vector  $(1, 1, 1)^t$  while  $F_{30}$  estimates the directional derivative in the direction of the vector  $(1, -1, -1)^t$ .

### C. The FAST Denoising Algorithm

Let  $\mathbf{X}$  represent a 3D volume of data and let  $\mathcal{DF}$  be the collection of all directional filters used for thresholding,  $\mathcal{DF} = \{F_1, F_3, F_9, F_{27}, F_{28}, F_{29}, F_{30}\}$ . Let  $Y_F = \mathbf{X} * F$ , where  $F \in \mathcal{DF}$  is one of the directional filters, and let  $\{Y_F\}_{F \in \mathcal{DF}}$  be the edge responses in all the directions considered. Our objective is to use the edge information we can obtain from thresholding these coefficients in order to reconstruct a denoised dataset.

We first estimate statistics for each direction. Let  $m_F, s_F$  be the mean and standard deviation, respectively, of the absolute values of all the coefficients in the  $F$  direction, where  $F \in \mathcal{DF}$ . We then set for each band a high threshold bound,  $T_2(F)$  ( $T_2(F) = m_F + s_F$ ) and low  $T_1(F)$  threshold bound ( $T_1(F) = m_F$ ) and outline a hysteresis affine thresholding strategy as follows. The function that implements affine thresholding is ( $T_2 > T_1 > 0$ ):

$$\rho_{T_1, T_2}(x) = \begin{cases} x & , \text{ if } |x| > T_2 \\ \frac{T_2}{T_2 - T_1}(x + \text{sgn}(x)T_1) & , \text{ if } T_1 < |x| \leq T_2 \\ 0 & , \text{ otherwise.} \end{cases}$$

If a coefficient's absolute value for the direction  $F$  exceeds  $T_2(F)$ , the coefficient is retained. If the absolute value is between  $T_1(F)$  and  $T_2(F)$ , to make the decision about retaining this coefficient we check all other directions for the coefficients that correspond to the same spatial location (voxel). If at least one more direction has absolute value above the lower threshold bound, the coefficient is retained.

$$\tilde{Y}_F = \begin{cases} \rho_{T_1(F), T_2(F)}(Y_F) & , \text{ if } ( |Y_F| > T_2(F) ) \text{ or} \\ & ( T_2(F) \geq |Y_F| > T_1(F) ) \\ & \text{and} \\ & \exists H \neq F : |Y_H| > T_1(H) \\ 0 & , \text{ otherwise} \end{cases} \quad (2)$$

In addition, we can recursively apply our thresholding scheme using the output of the  $\hat{K}_0$  filter (low-pass band)

as the new input. In summary, our FAST (Frames-based Adaptive hyStereSis Thresholding) algorithm operates as follows:

<i>Denoising algorithm : FAST</i>
Input : The noisy data $\mathbf{X}$ and the number of decomposition levels $L$ .
Step 1: Recursively decompose the volume $\mathbf{X}$ up to level $L$ using the filter bank defined in Table I to obtain $\mathbf{Y}_F$ .
Step 2: Compute $\tilde{\mathbf{Y}}_F$ by applying the ensemble approach described in Eq. 2.
Step 3: Reconstruct $\tilde{\mathbf{X}}$ from $\tilde{\mathbf{Y}}_F$ using the filter bank defined in Table I.

It should be noted that our ensemble approach to threshold frame coefficients is different from the classical wavelet thresholding approach. Our method takes advantage of multi-directional information. Our previous method [5] made distinction between directions by considering dual sets. This asks for a precedence order and leads to omitting voxels with acceptable filter response. We will capture these voxels by treating all directions as equally important.

### III. RESULTS AND DISCUSSION

We have tested our method on several confocal microscopy datasets. The neuron cells are either loaded with Alexa Fluor 555 and 488 dyes or taken from a line expressing enhanced green fluorescent protein. The current cells of interest are CA1 pyramidal cells from mice or rat hippocampi, and the original cell volume was de-convolved using Huygens<sup>TM</sup> software. These experimental datasets consist of three or more partially overlapping stacks with an approximate resolution of 1024x1024x149 each. A detail of such dataset is presented in Figure 2(i). The resolution is 0.230178  $\mu\text{m}$  in the  $x, y$  directions and 0.5  $\mu\text{m}$  in the  $z$  direction. Note that each stack may exhibit a different noise level with the effect that noise is not homogenous when the stacks are combined together.

We have compared our method to two others reported in the literature, *Bishrink* and *Median*, in addition to our previous method [5]. The *Bishrink* method implements a separable orthonormal 3D wavelet transform followed by bivariate shrinkage of the resulting coefficients, as described by Sendur and Selesnick [9]. The *Median* method uses a non-separable, non-linear median filter (mask size: 3x3x3).

To establish a quantitative assessment of our method compared to the other algorithms, we have created a synthetic volume dataset. Figure 2(a) depicts a volume with dimensions of 219x131x122 and with isotropic voxels. The volume was created starting with the morphology descriptions in the file n125.swc from the Duke-Southampton’s neuron database. This binary synthetic volume establishes the ground truth data for the comparison. We then corrupted this dataset using Poisson noise [7], denoised it using the three methods referenced above, and compared the reconstructed

TABLE II  
PERFORMANCE EVALUATION

Denoising Method	TPR	FPR	TNR	FNR	GM
FAST	97.54	0.66	99.34	2.64	98.44
Frames-based [5]	93.06	0.89	99.11	6.94	96.04
<i>Bishrink</i>	87.60	0.41	99.59	0.12	93.40
Median Filter	79.04	0.11	99.89	20.96	88.86

denoised volume voxel-wise to the ground truth. To obtain the binarization of the denoised volumes we used a maximum intensity threshold of 250 for the noise. Figures 1 and 2 are presented for visual inspection of the results. Figure 1 depicts the entire synthetic volume with noise, its maximum intensity projections and a detail. Figures 2(a)-(h) depict maximum intensity projections and a 3D detail of the denoised volumes. Visual inspection reveals that the FAST algorithm is more robust to speckle noise influence than the *Bishrink* algorithm, and that both of these algorithms preserve the morphology of the dendrites more faithfully than *median* filtering. Figures 2(i,j) depicts details of the real data and the same detail after denoising with FAST. Again, we note that our method results in more visually meaningful structures.

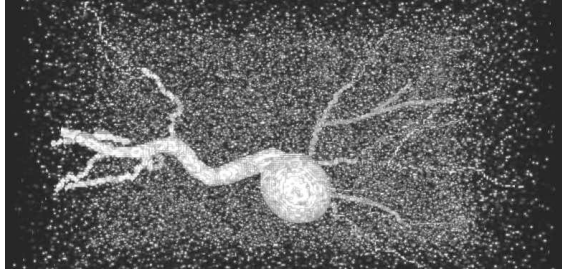
The comparison metrics used in this paper are the true positive rate (TPR), the false positive rate (FPR), the true negative rate (TNR), false negative rate (FNR), and the geometric mean (GM). These metrics are defined as follows: TPR is the proportion of voxels that were correctly identified to belong to the object of interest, FPR is the proportion of voxels that were incorrectly classified as the object of interest, TNR refers to the proportion of background voxels that were classified correctly, FNR is the proportion of object’s voxels that were incorrectly classified as background, and the GM is given by:  $\sqrt{TP \cdot TN}$ . Table II summarizes the results. All methods exhibit low FPR, a reflection of the fact that they are quite adept at identifying spurious artifacts. The poor performance of the median filtering method in terms of TPR reflects the fact that it fails to accurately preserve morphology and our algorithm achieves the highest TPR of almost 98%.

### IV. CONCLUSION

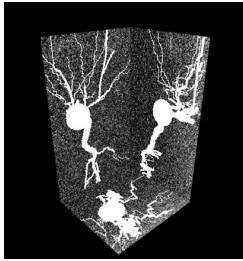
We have presented an improved method that allows us to denoise volume data from optical microscopy. It is based on a tight frame incorporating multidirectional edge detectors and it produces results that enable improved reconstruction. Although the results are presented in this application domain, our algorithms apply to any biomedical imaging data with similar assumptions about the sources of noise.

### REFERENCES

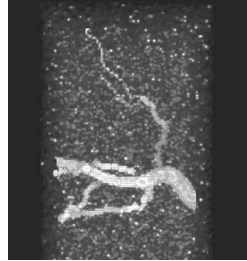
- [1] K.A. Al-Kofahi, S. Lasek, D.H. Szarowski, C.J. Pace, and G. Nagy. Rapid automated three-dimensional tracing of neurons from confocal image stacks. *IEEE Transactions on Information Technology in Biomedicine*, 6(2):171–187, June 2002.
- [2] P.J. Broser, R. Schulte, A. Roth, F. Helmchen, S. Lang, G. Wittum, and B. Sakmann. Nonlinear anisotropic diffusion filtering of three dimensional image data from two-photon microscopy. *Journal of Biomedical Optics*, 9(6):1253–1264, 2004.



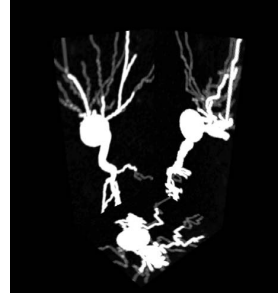
(a)



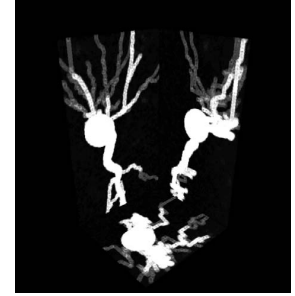
(b)



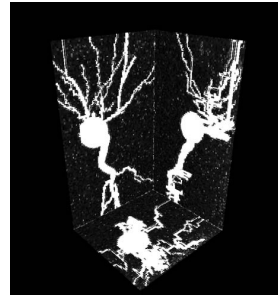
(c)



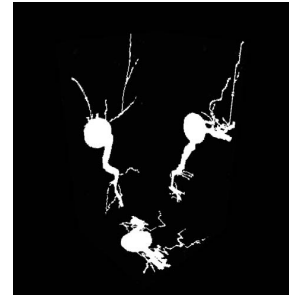
(a)



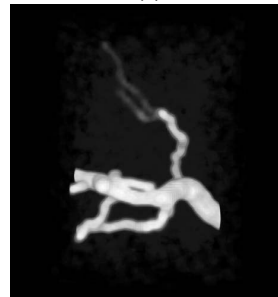
(b)



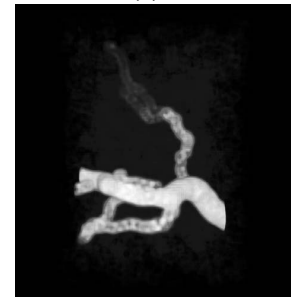
(c)



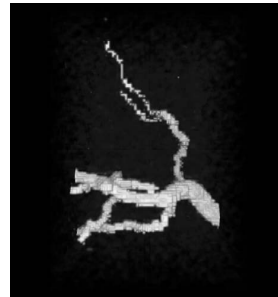
(d)



(e)



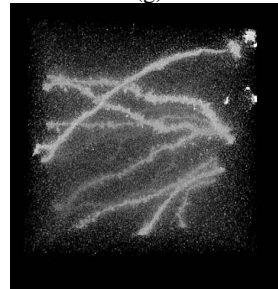
(f)



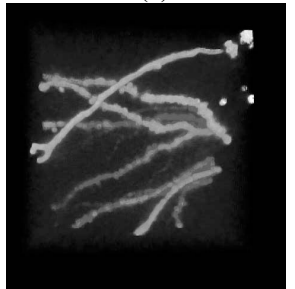
(g)



(h)



(i)



(j)

Fig. 1. (a) Synthetic volume, derived from n125.swc, with noise; (b) maximum intensity projections; (c) detail of the synthetic volume with noise.

- [3] A. Dima, M. Scholz, and K. Obermayer. Semi-automatic quality determination of 3D confocal microscope scans of neuronal cells denoised by 3D-wavelet shrinkage. *Proc. of the SPIE-Wavelet Applications VI*, volume 3723, pages 446–457, 1999.
- [4] A. Dima, M. Scholz, and K. Obermayer. Automatic segmentation and skeletonization of neurons from confocal microscopy images based on the 3-D wavelet transform. *IEEE Transactions on Image Processing*, 11(7):790–801, July 2002.
- [5] I. Konstantinidis, A. Santamaria, and I.A. Kakadiaris. Frames-based denoising in 3D confocal microscopy imaging. *Proc. 27th Annual International Conference of the IEEE Engineering in Medicine and Biology Society*, Shanghai, China, September 1-4, 2005.
- [6] M. Papadakis. *Sampling, Wavelets, and Tomography*, Chapter Generalized frame multiresolution analysis in abstract Hilbert spaces. Boston, 2003.
- [7] J.B. Pawley. *Handbook of Biological Confocal Microscopy*. Plenum, 1995.
- [8] A. Ron and Z. Shen. Affine system in  $L^2(\mathbf{R}^d)$ : the analysis of the analysis operator. *Journal of Functional Analysis*, 148:408–447, 1997.
- [9] L. Sendur and I.W. Selesnick. Bivariate shrinkage with local variance estimation. *IEEE Signal Processing Letters*, 9(12):438–441, December 2002.
- [10] L. Shen, M. Papadakis, I.A. Kakadiaris, I. Konstantinidis, D. Kouri, and D. Hoffman. Image denoising using a tight frame. *Proc. IEEE International Conference on Acoustics, Speech, and Signal Processing*, volume II, pages 641–644, 2005.

Fig. 2. Results on synthetic data with (a,e) FAST, (b,f) Frames-based [5], (c,g) *Bishrink*, and (d,h) median filtering; (i) detail of real data and (j) detail denoised with FAST.